Induced Fit and Kinetic Mechanism of Adenylation Catalyzed by *Escherichia coli* Threonyl-tRNA Synthetase†

Michael L. Bovee,‡ Melissa A. Pierce,§ and Christopher S. Francklyn*,‡

Department of Biochemistry, The University of Vermont Health Sciences Complex, Burlington, Vermont 05405-0068, and Saint Anselm College, Box 1828, 100 St. Anselm Drive, Manchester, New Hampshire 03102

Received September 2, 2003; Revised Manuscript Received October 21, 2003

ABSTRACT: Threonyl-tRNA synthetase (ThrRS) must discriminate among closely related amino acids to maintain the fidelity of protein synthesis. Here, a pre-steady state kinetic analysis of the ThRS-catalyzed adenylation reaction was carried out by monitoring changes in intrinsic tryptophan fluorescence. Stopped flow fluorimetry for the forward reaction gave a saturable fluorescence quench whose apparent rate increased hyperbolically with ATP concentration, consistent with a two-step mechanism in which rapid substrate binding precedes an isomerization step. From similar experiments, the equilibrium dissociation constants for dissociation of ATP from the E·Thr complex ($K_3 = 450 \pm 180$ μM) and threonine from the E·ATP complex ($K'_4 = 135$ μM) and the forward rate constant for adenylation ($k_{+5} = 29 \pm 4$ s^{-1}) were determined. A saturable fluorescence increase accompanied the pyrophosphorolysis of the E·Thr∼AMP complex, affording the dissociation constant for PP_i ($K_6 = 170 \pm 50$ μM) and the reverse rate constant ($k_{-5} = 47 \pm 4$ s^{-1}). The longer side chain of β-hydroxynorvaline increased the apparent dissociation constant ($K_{4[HNV]} = 6.8 \pm 2.8$ mM) with only a small reduction in the forward rate ($k'_{+5[HNV]} = 20 \pm 3.1$ s^{-1}). In contrast, two nonproductive substrates, threoninol and the adenylate analogue 5′-*O*-[*N*-(L-threonyl)sulfamoyl]-adenosine (Thr-AMS), exhibited linear increases in k_{app} with ligand concentration, suggesting that their binding is slow relative to isomerization. The proposed mechanism is consistent with steady state kinetic parameters. The role of threonine binding loop residue Trp434 in fluorescence changes was established by mutagenesis. The combined kinetic and molecular genetic analyses presented here support the principle of induced fit in the ThrRS-catalyzed adenylation reaction, in which substrate binding drives conformational changes that orient substrates and active site groups for catalysis.

The ability of aminoacyl-tRNA synthetases (aaRSs) to distinguish among closely related amino acids is essential for accurate protein synthesis. In the first phase of the two-step aminoacylation reaction, an aaRS will activate its amino acid substrate by condensation with ATP to form an enzyme-bound aminoacyl adenylate, and then transfer it to the 3′-terminal adenosine of its cognate transfer RNA (*1*, *2*). Remarkably, there are two distinct classes of aaRSs, each of which is characterized by a unique catalytic fold architecture, signature sequence motifs, and regiochemistry of aminoacylation (*3*−*5*). Unlike other biosynthetic enzymes, aaRSs face the special task of recognizing specific amino acid and transfer RNA substrates, as well as the universal substrate, ATP. How the aaRSs discriminate among closely related amino acids during the adenylation reaction remains a topic of continuing interest, particularly in light of efforts to expand the repertoire of amino acids inserted into proteins (*6*).

A number of aaRSs, such as TyrRS (*7*), AspRS (*8*, *9*), LysRS (*10*, *11*), and HisRS (*12*−*14*), are characterized by active sites that exploit the unique steric and chemical properties of their amino acid substrates, conferring the required accuracy of the cognate amino acid selection in one step, namely, the adenylation reaction. However, an aaRS that must discriminate between two amino acids that are isosteric, or differ by no more than a single methyl group, faces a more challenging task (*15*). As the first step toward achieving the low error rate of $\sim 10^{-4}-10^{-5}$ found in proteins, these enzymes employ pre- or post-transfer editing mechanisms to specifically reduce the inappropriate activation of noncognate amino acids. Such a mechanism was first demonstrated for isoleucyl-tRNA synthetase (*16*), where the difference in enzymatic efficiency (k_{cat}/K_M) for amino acid activation of isoleucine versus valine by IleRS is only 180-fold (*17*). This is even poorer than the overall error rate in protein synthesis of 1 in 3000 suggested in an earlier work that examined the rates of misincorporation of leucine and valine for isoleucine in ovalbumin (*18*). The editing mechanism employed by IleRS and the closely related enzymes ValRS and LeuRS relies on two distinct active sites, the first being responsible for the initial adenylate synthesis and the second devoted to the hydrolysis of misactivated and/or mischarged amino acids (*19*, *20*). Manipulation of the editing mechanisms employed by class I aaRSs has provided one of several approaches to engineering the incorporation of non-natural amino acids into proteins (*6*).

† This work was supported by National Institutes of Health Grants GM54899 and GM62491.

* To whom correspondence should be addressed. Phone: (802) 656-8450. Fax: (802) 862-8229. E-mail: franck@emba.uvm.edu.

‡ The University of Vermont Health Sciences Complex.

§ Saint Anselm College.

10.1021/bi0355701 CCC: $25.00
Published on Web 12/03/2003

Threonyl-tRNA synthetase (ThrRS) confronts a similar challenge in discriminating threonine from isosteric valine and chemically related serine. Recently determined crystal structures of complexes with cognate tRNA or a threonyl-adenylate analogue (*21*−*23*) show that ThrRS consists of a catalytic domain based on the characteristic class II fold, a C-terminal domain responsible for binding the tRNA anticodon, and an N-terminal extension (subdivided into domains N1 and N2) joined to the catalytic domain by a long α-helix. The selection of threonine by ThrRS is mediated by an essential pentacoordinately bound zinc ion in the active site that interacts with the threonine hydroxyl group, thereby promoting rejection of valine (*22*). Amino acid activation experiments indicate that the active site zinc and other active site residues of ThrRS provide a greater than 1000-fold preference for threonine over serine, but only a 70-fold preference for threonine over the non-natural amino acid β-hydroxynorvaline (*22*). While the extent of specificity for threonine over serine manifested by ThrRS at the level of adenylation is greater than that exhibited by IleRS in the selection of isoleucine over valine, it is not sufficient to accommodate the accuracy required for protein synthesis. Consistent with this view, it was subsequently shown that the ThrRS N-terminal extension contains an editing site that serves to hydrolyze misacylated serine by use of a post-transfer editing mechanism (*23*). When this domain is deleted, the editing function is abolished and the level of aminoacylation is decreased, but adenylation of threonine is virtually unaffected (*22*, *23*). Other class II enzymes for which editing functions have been reported include ProRS (*24*, *25*) and, by virtue of its homology with ThrRS over parts of the editing domain, AlaRS (*21*, *26*).

The most detailed picture of the adenylation reaction has been provided by the use of rapid kinetics, coupled with analysis of relevant crystal structures. In particular, pre-steady state kinetics experiments conducted on both *Bacillus stearothermophilus* and human TyrRS provided direct estimates of the energetic contributions of individual enzyme−substrate contacts (*27*−*32*). Other class I aaRS systems on which pre-steady state kinetic analyses have been performed include IleRS (*33*−*36*), TrpRS (*37*−*39*), MetRS (*40*), and ValRS (*41*). The work on the tyrosyl systems, as well as that on other systems, has contributed to the prevailing view that catalysis by the aaRS depends significantly on the development of binding energy between the enzyme and the transition state, with little contribution from covalent and acid/base catalysis. In contrast, pre-steady state kinetic analysis of amino acid activation by class II systems has been less extensive, with only limited work reported in the PheRS (*42*) and LysRS (*43*) systems. Insights into the mechanism of adenylate formation have been largely deduced from crystallographic analyses of SerRS (*44*), HisRS (*13*, *45*), and AspRS (*9*). By analogy to that of class I enzymes, catalysis appears to be promoted through the development of binding energy to the transition state. However, class II enzymes appear to share the common feature of stabilization of the presumed pentacoordinate α-phosphate transition state by a coordinated metal ion or a basic residue, which is not seen in class I enzymes (*46*). Here, we have applied pre-steady state kinetics to the study of the class II ThrRS from *Escherichia coli*. The results from these experiments show that the adenylation reaction is best described as a two-step mechanism in which a fast binding step is followed by a slower, isomerization step associated with induced fit conformational changes in the active site.

MATERIALS AND METHODS

Chemicals and Reagents. The nonhydrolyzable adenylate analogue 5′-*O*-[*N*-(L-threonyl)sulfamoyl]adenosine was synthesized by B. Sproat (RNA-TEC, Leuven, Belgium) and generously provided by A.-C. Dock-Brégeon (IGBMC, Illkirch, France). Amino acids and amino acid analogues were purchased from Sigma and Fluka. β-Hydroxynorvaline has previously been described as a specific threonine antagonist (*47*). Pyrophosphatase was obtained from Roche Molecular Biochemicals. Nucleotides were purchased from Amersham Biosciences. Radiolabeled [^{32}P]pyrophosphate was purchased from Perkin-Elmer Life Sciences. Ni−NTA agarose was purchased from Qiagen.

ThrRS Overexpression and Purification. *E. coli* threonyl-tRNA synthetase (ThrRS) was overexpressed in *E. coli* strain IBPC6881 transformed with plasmid pTetthrSΔHtag1, which encodes the enzyme with a C-terminal hexahistidine tag. The chromosomal copy of the *thrS* gene was insertionally inactivated by a kanamycin resistance cassette (*48*). This ensured that all ThrRS arose from the plasmid-borne *thrS* gene, which simplified purification and confirmed enzymatic function of the ThrRS mutant. The transformed *E. coli* strain was grown at 34 °C in LB medium supplemented with 10 μg/mL tetracycline, and *thrS* was under continuous induction with 0.5 mM IPTG. Bacteria were harvested by centrifugation after 6 h and lysed by sonication in low-ionic strength buffer A [25 mM Tris (pH 8) at 4 °C, 50 mM KCl, 5 mM $MgCl_2$, and 3 mM DTT]. The lysate soluble fraction was isolated by centrifugation at 10000*g*, and nucleic acids were further precipitated from the soluble fraction by dropwise addition of protamine sulfate to a final concentration of 0.1%, followed by centrifugation. The resulting supernatant was incubated with 5 mL of Ni−NTA affinity resin in batch mode in buffer B (buffer A with 20 mM imidazole) to bind ThrRS specifically, and then transferred to a 5 mL polypropylene column. Other proteins were removed by exhaustively washing the resin with buffer B. Pure ThrRS was eluted from the column in buffer C (buffer A with 150 mM imidazole), dialyzed into buffer D [20 mM Tris (pH 7.5), 150 mM KCl, and 15 mM $MgCl_2$], and then stored on ice prior to use in experiments.

Stopped Flow and Steady State Fluorescence Measurements. Steady state measurements were taken using a Photon Technology International (Lawrenceville, NJ) spectrofluorimeter equipped with a water-cooled 150 W xenon arc lamp. Samples were analyzed in a 0.4 cm × 1 cm quartz cuvette, using a 4 nm excitation bandwidth (290 ± 2 nm), and emission was collected above 320 nm by using a WG320 high-pass filter. Steady state fluorescence assays were performed in buffer D by titrating substrates over a range estimated from 0.2 to 5 times the dissociation constant into enzyme at a concentration of 0.25−1 μM (calculated as dimer). Intrinsic tryptophan fluorescence of the WT[1] and W434Y ThrRS enzymes was measured by wavelength

[1] Abbreviations: Thr, threonine; HNV, β-hydroxynorvaline; Thr∼AMP, threonyl-adenylate; Thr-AMS, 5′-*O*-[*N*-(L-threonyl)sulfamoyl]-adenosine; WT, wild type.

scanning to determine the optimal fluorescent yield for unliganded and liganded species in the presence or absence of varying concentrations of substrate. In the steady state experiments, fluorescence measurements were multiplied by $V_{final}/V_{initial}$ to correct for dilution, and normalized to unity at $[S]_0$ for titrations of the substrate (F_{thr}) or equal volumes of water (F_{water}). The substrate specific component of the fluorescence quench was determined by addition of a correction factor, $1 - F_{water}$, to each corresponding F_{thr} measurement in the titration. Transient state fluorescence measurements were taken using a MOS-250 spectrophotometer with fiber optic excitation and emission connected to a μSFM-20 flow module, both manufactured by Biologic (Claix, France). Excitation was at 290 ± 2.5 nm, and emission was collected using a WG320 high-pass filter as described above. The instrument dead time was approximately 2 ms. In a typical experiment for measuring the rate of the forward reaction, one syringe contained ThrRS (0.5 μM), pyrophosphatase (0.5 unit/mL), and saturating concentrations of threonine (10 mM) or Mg·ATP (10 mM). The variable syringe contained pyrophosphatase, 0.2−10 mM threonine or 0.2−10 mM Mg·ATP, and the same saturating concentration of the other substrate as described above. All reactions were conducted in buffer D. Individual reaction mixtures received equal volumes (39 μL) from each syringe, and the fluorescence decrease (or increase) was monitored over 5 s. For experiments in which the reverse reaction was assessed, one syringe contained the preformed E·Thr∼AMP complex (1 μM) that had been separated from free substrates while the second contained tetrasodium pyrophosphate (0.02−2.0 mM). Pre-steady state initial fluorescence values were determined for each experiment by rapidly mixing the same enzyme preparation with buffer lacking only the indicated substrate.

Data Analysis. For each reaction, up to 10 raw data traces were averaged. Apparent rate constants were determined using the Biokine software package version 3.25, in which data were fit to a form of eq 1:

$$y = at + b + c(e^{-kt}) \quad (1)$$

where y is the fluorescence intensity, a is the baseline slope, b is the offset, c is the amplitude, k is the apparent rate constant, and t is the independent variable, time. Error bars in k_{app} versus [S] plots indicate the 95% (±2 standard deviations) confidence limit unless otherwise indicated.

Equilibrium Dialysis. Experiments were performed in a five-cell microdialyzer apparatus (Spectrum Laboratories, Rancho Dominquez, CA). Concentrated enzyme stocks were dialyzed at 4 °C into 50 mM Tris (pH 7.5), 50 mM NaCl, 10 mM $MgCl_2$, and 1 mM β-mercaptoethanol. Sample volumes of 125 μL containing either enzyme (25 μM) or [^{3}H]threonine (10−1000 μM, specific activity of 50−75 cpm/pmol) were loaded into opposing sides of a semipermeable membrane and incubated overnight at 4 °C with continuous slow rotation. Artifacts due to surface adsorption effects were controlled by equilibrating the amino acid from either direction. Measurement of the radioactivity present in both chambers at equilibrium by scintillation counting allowed the concentrations of free and of bound + free threonine to be determined at each ligand concentration. Bound was calculated by subtracting free from bound + free. Data were plotted as bound versus free (hyperbolic plot, eq 2) and bound/free versus bound (Scatchard linear transform plot, eq 3).

$$[Thr]_{bound} = \frac{[Thr]_{free} \times n[E]_{total}}{[Thr]_{free} + K_D} \quad (2)$$

$$\frac{[Thr]_{bound}}{[Thr]_{free}} = -\frac{1}{K_D}[Thr]_{bound} + \frac{n[E]_{total}}{K_D} \quad (3)$$

where $[Thr]_{bound}$ is the concentration of threonine bound to ThrRS, $[Thr]_{free}$ is the concentration of unbound threonine at equilibrium, n is the number of independent binding sites per enzyme dimer, $[E]_{total}$ is the enzyme concentration, and K_D is the equilibrium dissociation constant for threonine.

Steady State Pyrophosphate Exchange Kinetics. The steady state parameters k_{cat} and K_M for both threonine and ATP were determined by the pyrophosphate exchange assay, as described previously (*22*). In contrast to the previous study, a higher fixed concentration of ATP (5 vs 2 mM) was used for assays in which the threonine concentration was varied. Pyrophosphate exchange kinetics were also carried out with a fixed threonine concentration (5 mM) and varying Mg·ATP (135 μM to 5 mM), allowing determination of an apparent K_M for ATP and k_{cat} for exchange.

RESULTS

Fluorescence Changes Associated with the Adenylation Reaction. The stopped flow analysis described below was analyzed according to Scheme 1, which serves as a minimal mechanism for ThrRS-catalyzed adenylation. The transient kinetic and steady state kinetic data obtained can be described using the rate and equilibrium constants presented in Scheme 1 and Table 1. The convention for the various rate and equilibrium constants is that described previously by Pope *et al*. (*34*), and defined explicitly in Table 1. Equilibrium or dissociation constants are given as K_n, while elementary rate constants are given as k_{+i} or k_{-i}.

Scheme 1

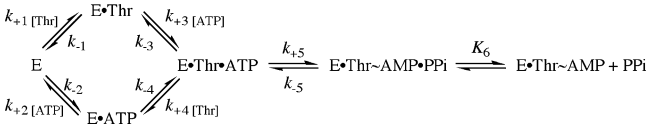

The addition of increasing concentrations of threonine to a fixed concentration of ThrRS under steady state conditions led to a quench of tryptophan fluorescence on the order of 5%, but no transient was detected under stopped flow conditions (data not shown). A similar steady state fluorescence quench may be associated with ATP binding by ThrRS, but likewise could not be reliably quantitated. When ATP is rapidly mixed with ThrRS saturated with threonine (herein termed E·Thr), a single-exponential quench with a 6% amplitude is observed with a $t_{1/2}$ of ≈25 ms (Figure 1A). When increasing concentrations of Mg·ATP were rapidly mixed with E·Thr, k_{app} increased hyperbolically, and the rate of the fluorescence change exhibited no dependence on enzyme concentration over the range from 0.2 to 2.0 μM. This response is consistent with a two-step kinetic mechanism in which the formation of a bimolecular complex is

Table 1: Rate Constants for Substrate Binding, Activation, and Inhibitor Binding to *E. coli* ThrRS[a]

reaction step	rate/equilibrium constant[b]	basis for parameter
E + Thr ⇌ E·Thr	$K_1 = 215\ \mu M$	equilibrium dialysis
E + ATP ⇌ E·ATP	$K'_2 = 717\ \mu M$	estimate from $(K_1K_3)/K_4$
E·Thr + ATP ⇌ E·Thr·ATP	$K_3 = 450 \pm 180\ \mu M$	midpoint of Figure 1B
E·ATP + Thr ⇌ E·ATP·Thr	$k_{+4} = 2.4 \times 10^4\ M^{-1}\ s^{-1}$	slope of Figure 1C
E·ATP·Thr ⇌ E·ATP + Thr	$k_{-4} = 3.2\ s^{-1}$	intercept of Figure 1C
E·ATP + Thr ⇌ E·ATP·Thr	$K'_4 = 135\ \mu M$	derived from k_{-4}/k_{+4}
E·ATP + HNV ⇌ E·ATP·HNV	$K_{4[HNV]} = 6.8 \pm 2.8\ mM$	midpoint of Figure 3A
E·Thr·ATP ⇌ E·Thr∼AMP + PP_i	$k_{+5} = 29 \pm 4.0\ s^{-1}$	limit value of Figure 1B
E·HNV·ATP ⇌ E·HNV∼AMP + PP_i	$k_{+5[HNV]} = 20 \pm 3.1\ s^{-1}$	limit value of Figure 3A
E·Thr∼AMP + PP_i ⇌ E·Thr·ATP	$k_{-5} = 47 \pm 4.1\ s^{-1}$	limit value of Figure 4B
E·Thr∼AMP + PP_i ⇌ E·Thr∼ATP	$K_6 = 170 \pm 50\ \mu M$	midpoint of Figure 4B
E·ATP + ThrOH ⇌ E·ATP·ThrOH	$k_{on} = (2.3 \pm 0.2) \times 10^4\ M^{-1}\ s^{-1}$	slope of Figure 3B
E·ATP·ThrOH ⇌ E·ATP + ThrOH	$k'_{off} = 19\ s^{-1}$	$[k_{app}(k_{fwd} + k_{rev})]/k_{rev}$ (eq 5)
E·ATP·ThrOH ⇌ E·ATP + ThrOH	$K'_{ThrOH} = 830\ \mu M$	k'_{off}/k_{on}
E + Thr-AMS ⇌ E·Thr-AMS	$k_{on} = (1.6 \pm 0.2) \times 10^5\ M^{-1}\ s^{-1}$	slope of Figure 3C
E·Thr-AMS ⇌ E + Thr-AMS	$k'_{off} = 0.3\ s^{-1}$	$[k_{app}(k_{fwd} + k_{rev})]/k_{rev}$ (eq 5)
E + Thr-AMS ⇌ E·Thr-AMS	$K'_{Thr-AMS} = 2\ \mu M$	k'_{off}/k_{on}

[a] E is ThrRS. [b] Parameters denoted with a prime are estimates derived as indicated in the text.

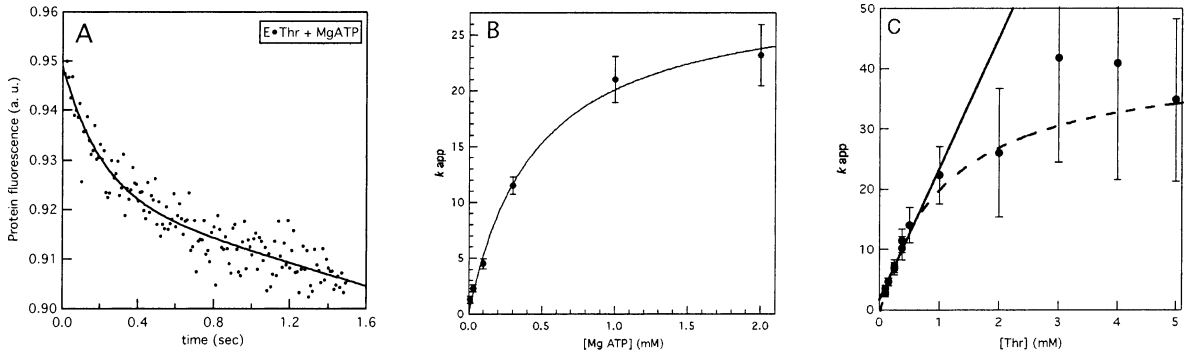

FIGURE 1: Protein fluorescence changes that occur upon combining adenylation reactants with enzyme. All reactions were carried out in the stopped flow apparatus using the standard buffer and temperature conditions described in Materials and Methods. Enzyme and threonine concentrations were 2 μM and 10 mM, respectively, before they were mixed in a 1:1 ratio in the reaction mixture with ATP. (A) Rapid mixing of E·Thr with 60 μM Mg·ATP. The curved line is the best fit to eq 1. (B) Stopped flow titration of ATP with the E·Thr complex. The solid line is the best fit using eq 4. (C) Stopped flow titration of threonine with the E·ATP complex. The dashed line is the best fit to eq 4. The solid line represents a linear least-squares fit to the initial linear portion of the curve, assuming a breakdown of the rapid equilibrium assumption (*49*, *53*).

followed by a unimolecular isomerization step, according to Scheme 2.[2]

Scheme 2

$$\text{E·Thr} + \text{ATP} \underset{k_{-3}}{\overset{k_{+3[ATP]}}{\rightleftharpoons}} \text{E·Thr·ATP} \underset{k_{-5}}{\overset{k_{+5}}{\rightleftharpoons}} [\text{E·Thr·ATP}]^*$$

For a two-step mechanism, a maximum of two relaxations can be observed (*49*). In the experiment described above, only one transient was observed. One of at least three explanations may account for this. First, there may in fact be two fluorescence changes (relaxations) upon mixing ATP with E·Thr that are well separated with respect to rate, but the first occurs within the dead time of the instrument. Alternatively, the two putative relaxation times may be too close to one another to be decoupled, or only one fluorescence change occurs, and is specific to the isomerization step.

To distinguish among these different interpretations, we note that the fluorescence decrease observed with threonine alone was 5%, while the decrease associated with rapidly mixing threonine and ATP together into ThrRS was 10%. Moreover, in transient experiments where unliganded ThrRS was mixed with threonine and ATP simultaneously, nearly half of the amplitude occurred in the dead time of the instrument, and amplitudes could not be reliably estimated when the concentration of either substrate was varied. Accordingly, the preferred interpretation is that a fast fluorescence change ($k_{app} > 250-300\ s^{-1}$) reflecting the initial encounter of ATP with E·Thr occurs within a few milliseconds of mixing, and is followed by a second, slower transient. By employing the simplifying assumption that the first step is fast relative to the second, and restricting the experimental conditions to a large substrate excess, we analyzed the rate of the transient quench as follows

$$k_{app} = \frac{k_{+5}[S]_0}{K_3 + [S]_0} + k_{-5} \quad (4)$$

where K_3 is the apparent dissociation constant for dissociation of ATP from the E·Thr complex and k_{+5} and k_{-5} represent the forward and reverse rate constants, respectively, for the isomerization of E·Thr·ATP to [E·Thr·ATP]*. Figure 1B displays the resulting plot of k_{app} versus [ATP], from which the values of 450 ± 180 μM and 29 ± 4 s^{-1} were obtained for K_3 and the limiting value for $k_{+5} + k_{-5}$, respectively. Here, a y intercept of $<1\ s^{-1}$ suggests that the value for k_{-5}

[2] For clarity, the rate constants designated in Scheme 1 will be maintained throughout the paper.

is not reliably determined. This is likely due to the inclusion of pyrophosphatase in the reaction, or the relatively weak binding of pyrophosphate (PP_i) to the enzyme−adenylate complex (*34*, *50*). Thus, the limiting value of 29 s^{-1} for k_{app} can be taken to be a reasonable estimate of k_{+5}, the forward rate of isomerization. A similar limiting value of 29 s^{-1} was observed in pre-steady state experiments in which unliganded ThrRS was rapidly mixed with threonine and ATP without preincubation (data not shown). The value of 450 μM for K_3 is within a factor of 2 of the Michaelis constant for ATP in the pyrophosphate exchange reaction (see below and ref *22*). Accordingly, a two-step mechanism in which a relatively fast ATP binding step is followed by a slow isomerization step appears to account plausibly for the observations.

The effect of reversing the order of substrate addition was examined by titrating threonine into the preformed E·ATP complex. As in the previous experiment, the observed rate constant can be interpreted as a hyperbolic dependence on increasing concentrations of the variable substrate [Figure 1C (− − −)]. A fit of the data to eq 4 returned values of 1.2 ± 0.6 mM for K_4, the apparent dissociation constant for dissociation of threonine from the E·ATP complex, and a value of 47 ± 9 s^{-1} for k_{+5}. The saturating value of k_{app} is nearly double the rate observed when ATP is the variable substrate, while the apparent value of K_4 estimated from the midpoint of the plot is at least 10-fold higher than the K_M for threonine determined from steady state kinetics (*22*). As we will develop below (see Discussion), these discrepancies are likely a reflection of the breakdown of the rapid equilibrium assumption ($k_{+4}[S] + k_{-4} \gg k_{+5} + k_{-5}$) when ATP binding precedes threonine binding.

Threonine Analogues in the Adenylation Reaction. The observation of a two-step mechanism in the forward reaction raises two distinct possibilities. The unimolecular step immediately following binding may reflect the chemical step in which the adenylate is formed, or represent a conformational change in the E·S complex that precedes chemistry, as seen in the myosin ATPase mechanism (*51*). To distinguish between these possibilities, pre-steady state experiments were performed using the threonine analogues β-hydroxynorvaline (β-HNV) and threoninol (ThrOH), as well as the adenylate product analogue 5′-*O*-[*N*-(L-threonyl)-sulfamoyl]adenosine (Thr-AMS). The structures of these compounds are shown in Figure 2. The analogue β-hydroxynorvaline differs from threonine by the replacement of the side chain methyl group with an ethyl group, resulting in a 17-fold increased K_M relative to that of threonine in the pyrophosphate exchange reaction (*22*). (In contrast, neither threoninol nor Thr-AMS is a productive substrate for the adenylation reaction.) Like threonine, rapid mixing of β-HNV with the preformed E·ATP complex was accompanied by a 5% fluorescence quench that was described well by a single exponential with a $t_{1/2}$ of ≈25 ms (data not shown). As in the case of threonine, the k_{app} for this reaction exhibited a hyperbolic dependence on increasing β-HNV concentration, with values of 6.8 ± 2 mM and 20 ± 3 s^{-1} for the apparent dissociation constant (K'_{HNV}) and saturating value of k_{+5}, respectively (Figure 3A). Notably, the difference between β-HNV and threonine appears to be confined to changes in the apparent dissociation constant, although the magnitude of the increase in K'_{HNV} was smaller than that observed for K_M in the steady state kinetics (*22*). Thus, β-HNV appears to be rejected by virtue of weak binding during the formation of the bimolecular complex, rather than during the isomerization step.

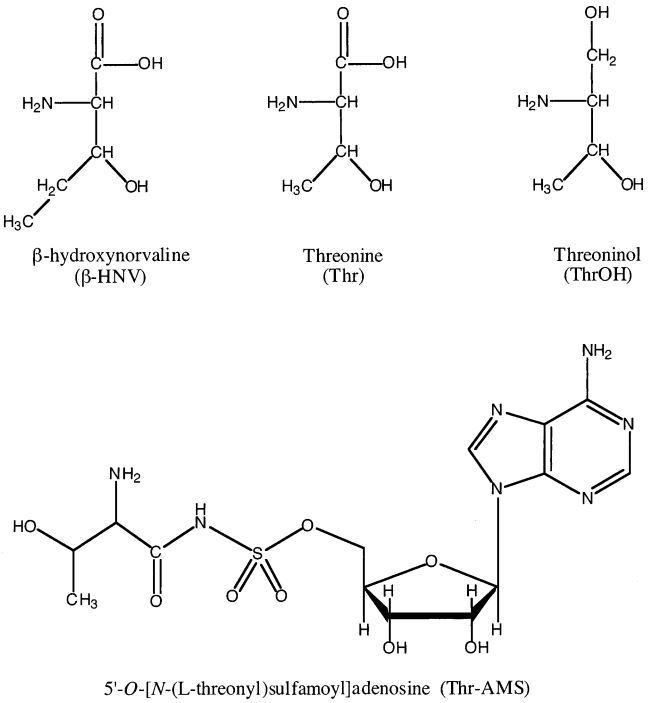

FIGURE 2: Comparison of the structures of relevant amino acid substrates and analogues. Threonine analogue β-hydroxynorvaline and cognate threonine are competent substrates for adenylation. Threoninol and the nonhydrolyzable adenylate analogue Thr-AMS bind to the enzyme active site but do not participate in catalysis.

In contrast to β-hydroxynorvaline, which exhibited a hyperbolic response of k_{app} to increasing analogue concentrations, the nonreactive analogues threoninol and Thr-AMS both exhibited linear dependences on increasing ligand concentrations (Figure 3B,C). The linear response can be explained by one of two models, the first being a simple bimolecular interaction. As these experiments were carried out under conditions of considerable substrate excess, these reactions represent a pseudo-first-order transformation of E (or E·ATP) into E·Thr-AMS or E·ATP·ThrOH. Plots of k_{app} versus [S] yielded k_{on} values of (2.3 ± 0.2) × 10^4 M^{-1} s^{-1} for the bimolecular association constant of threoninol (Figure 3B, slope) and (1.6 ± 0.2) × 10^5 M^{-1} s^{-1} for Thr-AMS (Figure 3C, slope). In this simple bimolecular interaction model, the *y* intercept is the unimolecular dissociation constant (k_{off}), and a value of 12 ± 4 s^{-1} was returned for threoninol. The *y* intercept in the case of Thr-AMS was 0.2 ± 4.5 s^{-1}, too close to zero to be reliably determined from the plot, but an estimate of ≈1 s^{-1} was taken as an upper bound. On the basis of these elementary rate constants, the corresponding equilibrium dissociation constants ($K_D = k_{off}/k_{on}$) were estimated to be 520 μM for threoninol and 1 μM for Thr-AMS.

While the bimolecular (single-step) model is the simplest interpretation of the stopped flow data, it is not necessarily the best. In accord with structural evidence that will be reviewed below (see Discussion), the binding of threoninol to E·ATP or the binding of Thr-AMS to free enzyme may also be interpreted in the context of a two-step mechanism (Scheme 3). In this scheme, a linear dependence of k_{app} on

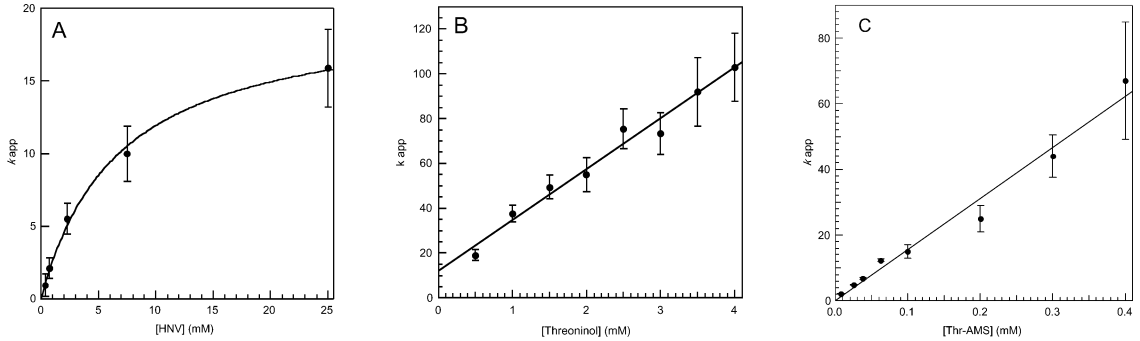

FIGURE 3: Concentration dependence of k_{app} on the binding of substrate analogues to ThrRS. The enzyme concentration was 0.25 μM in the reaction mixture, and the final MgATP concentration was 3 mM where present. (A) β-HNV titration against the E·ATP complex. The curved line is a fit to eq 4, with the simplifying assumption that $k_{-2} = 0$. (B) Titration of threoninol against E·ATP. The straight line is the best linear least-squares fit of all data points. (C) Titration of Thr-AMS with unliganded ThrRS. The straight line is the best linear least-squares fit of all data points. Error bars in panels B and C denote the standard deviation.

Scheme 3

$$E + S \underset{k_{off}}{\overset{k_{on}}{\rightleftharpoons}} ES \underset{k_{rev}}{\overset{k_{fwd}}{\rightleftharpoons}} [ES]^*$$

substrates would be predicted if a fluorescence quench in ThrRS were restricted to the initial binding event, with no changes in protein fluorescence accompanying the subsequent isomerization. This possibility is deemed unlikely, because the presumptive conformational changes that occur in response to both productive and unproductive substrates are likely to be similar, as the final states are identical (see Discussion). Alternatively, the linear response can be rationalized by a model in which the initial bimolecular interaction is slow relative to the isomerization step (*49*). Two transients would also be predicted in this model, but unlike the case proposed for the productive substrates (fast binding followed by slow isomerization), the fast relaxation ($1/\tau_1$) is equal to $k_{fwd} + k_{rev}$ while the slow relaxation ($1/\tau_2$) includes contributions from all four elementary rate constants.[3]

$$k_{app} = \frac{1}{\tau_2} = k_{on}[E+S] + \frac{k_{off}k_{rev}}{k_{fwd} + k_{rev}} \qquad (5)$$

Both the simple bimolecular and the slow binding and fast isomerization models make the same prediction about the slope (i.e., equivalent to k_{on}), but different predictions about the *y* intercept. Significantly, transient experiments using threoninol and Thr-AMS exhibited the same rapid fluorescence decrease in amplitude during the dead time that was seen for the productive substrates, which could represent a transient too fast to measure accurately. Along with structural results reviewed below (see Discussion), this observation provides support for a two-step mechanism in which the isomerization step may be faster than the initial binding encounter with the ligand. For both productive and nonproductive substrates, substrate binding is always followed by a conformational change that may significantly contribute to the fluorescence change. The important distinction is that the conformational change may be concerted with respect to chemistry for productive substrates, leading to a slower rate of isomerization. For the nonproductive substrates, where no chemistry occurs, the isomerization rate should be faster.

As a consequence of our inability to resolve the proposed fast transient, it is not possible to measure $1/\tau_1$ ($=k_{fwd} + k_{rev}$), preventing the direct determination of k_{off}, k_{fwd}, and k_{rev} from the *y* intercept. However, an estimate of the dissociation rate constants (k_{off}) for threoninol and Thr-AMS can be made by use of the values of k_{+5} (determined from the titrations above) and k_{-5} (determined below) from experiments with productive substrates. On the basis of the assumption that isomerization is likely to be faster for nonproductive substrates, k_{+5} and k_{-5} are almost certain to be considerable *underestimates* of k_{fwd} and k_{rev}. By inserting into eq 5 the *y* intercepts (k_{app}) from panels B and C of Figure 3 and the estimates of 29 and 47 s^{-1} as lower bounds on k_{fwd} and k_{rev}, respectively, we estimated dissociation rates (k'_{off}) for threoninol and Thr-AMS of 19 and 0.3 s^{-1}, respectively. From these dissociation rates, revised estimates of the equilibrium dissociation constants (calculated as k'_{off}/k_{on}) were 830 μM for K'_{ThrOH} and 2 μM for $K'_{Thr-AMS}$ (Table 1).

Fluorescence Changes Associated with Pyrophosphorolysis, the Reverse of the Adenylation Reaction. The results described above suggest that the fluorescence quenches associated with the productive forward adenylation reaction reflect rapid, random binding of both cognate substrates followed by a slower isomerization that may be concerted with respect to chemistry. Accordingly, reversing the adenylation reaction should produce a fluorescence change equal in amplitude to but opposite in sign from that observed in the forward reaction. To examine the reverse reaction, the E·Thr∼AMP complex was formed, separated from unreacted substrate, and then mixed with increasing concentrations of sodium pyrophosphate under stopped flow conditions. As shown in Figure 4A, a transient fluorescence increase is observed under these conditions. The rate of this transient increased with increasing Mg·PP_i concentration, reaching a plateau at 47 $\pm$ 4.1 s^{-1}. The apparent equilibrium dissociation constant for pyrophosphate (K'_{PP_i}) derived by fitting the data to the appropriate version of eq 4 was 170 $\pm$ 50 μM (Figure 4B). Titrations at higher pyrophosphate concentrations were precluded by the formation of a precipitate under experimental conditions. The fluorescence increase observed during the reverse reaction restores the signal to the same level as the unliganded enzyme, suggesting that the low concentrations of ATP and threonine formed by reversal of the reaction

[3] Note that in this model k_{fwd} and k_{rev} for the nonproductive substrates are analogous to k_{+5} and k_{-5}, respectively, for the productive substrates. The rate constants k_{on} and k_{off} are analogous to k_{+3} and k_{-3} or k_{+4} and k_{-4}, respectively.

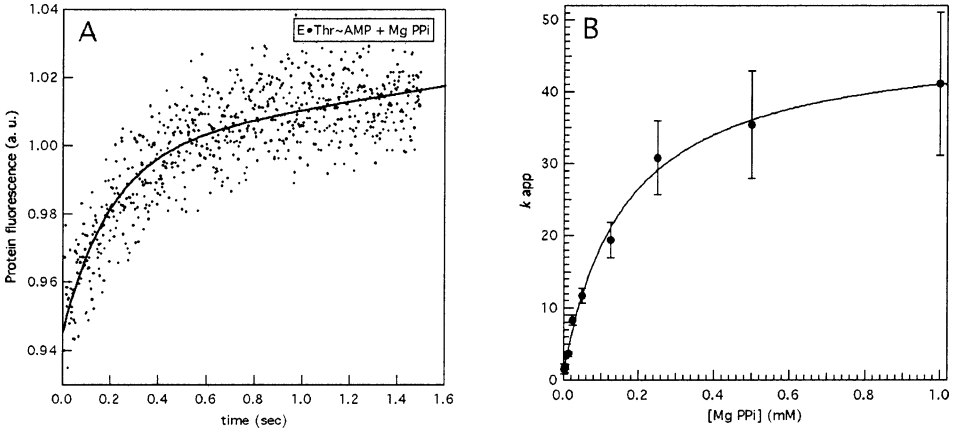

FIGURE 4: Reaction of the ThrRS−adenylate complex with magnesium pyrophosphate. (A) Transient fluorescence increase upon mixing 1 μM E·Thr~AMP with 25 μM Mg·PP$_i$. The complex was prepared as described in Materials and Methods. The curved line was fit using eq 1. (B) Pyrophosphate titration with E·Thr~AMP. The curved line was fit using eq 4.

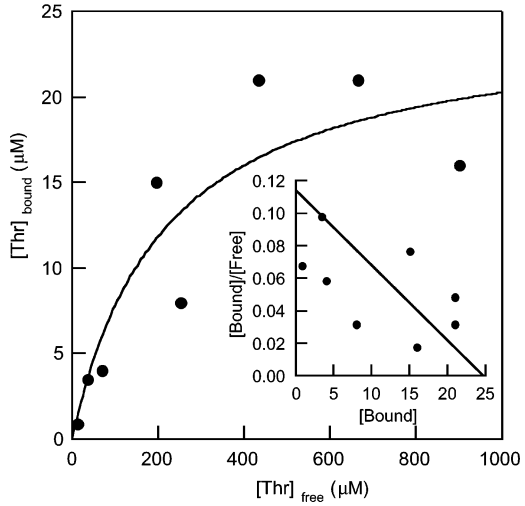

FIGURE 5: Equilibrium dissociation constant for threonine binding to ThrRS determined by equilibrium dialysis. ThrRS (25 μM) was dialyzed against various [^{3}H]threonine concentrations. Binding was quantitated by scintillation counting, and plots were generated from a collection of data points from three independent experiments as described in Materials and Methods. The inset is a Scatchard linear transform. The *x* intercept equals the total concentration of binding sites (B_{max}); the *y* intercept = B_{max}/K_D, and the slope = $-1/K_D$.

are too low to favor detectable rebinding to the enzyme. The hyperbolic dependence of k_{app} on [PP$_i$] is once again consistent with a two-step mechanism. In this case, the rapid binding of pyrophosphate is followed by regeneration of threonine and ATP from the bound threonyl-adenylate, which may then freely diffuse from the active site.

Quantitative Analysis of Threonine Binding by Equilibrium Dialysis. Fluorescence changes alone provide only indirect information about the physical nature of the events they report, and their interpretation is entirely mechanism dependent. Therefore, at least one complementary method for measuring fundamental kinetic parameters independent of a specific mechanism was used to bolster interpretation of the results. To this end, the apparent dissociation constant and binding stoichiometry for threonine were measured directly using equilibrium dialysis, as described in Materials and Methods. Figure 5 shows a binding isotherm fit by nonlinear regression over a range of threonine concentrations, and a fixed enzyme concentration of 25 μM. The results indicate an apparent K_D (equivalent to K_1 in Scheme 1) of 215 μM, 4-fold lower than the value of K_3 determined by transient kinetic analysis, but within a factor of 2 of the value of K_{ThrOH} determined above. Although the enzyme concentration was well below K_D, the stoichiometry of threonine binding appears to be 1 mol per mole of enzyme homodimers (B_{max} = 25 μM). Thus, ThrRS is able to bind threonine in the absence of ATP, yet with a stoichiometry of one molecule per dimer. These data do not preclude the possibility that concentrations of threonine greater than the range tested (10 μM to 1 mM) might lead to occupancy of the second active site on the dimer, producing a stoichiometry of two. (Data at these higher concentrations were not experimentally accessible, because of the prohibitive concentrations of enzyme required.) Interestingly, these results are consistent with crystallographic analysis of the complex of the N-terminal domain of truncated ThrRS with threonine, which also exhibited a stoichiometry of one threonine bound per dimer (*22*).

Trp434 Is a Significant Component of the Threonine-Dependent Fluorescence Quench. Changes in protein fluorescence are a reflection of changes in the chemical environment of one or more tryptophan residues. Each subunit of the ThrRS dimer possesses 11 tryptophans (*52*) distributed among the three principal structural domains. On the basis of their proximity to the binding sites for threonine and ATP, Trp434 and Trp478 were selected for substitution with tyrosine by site-directed mutagenesis. While both changes were readily incorporated into the plasmid-borne *thrS* gene, only the W434Y ThrRS mutant resulted in the accumulation of a stable enzyme that could be readily purified and characterized. Moreover, the W434Y mutant was capable of complementing a *thrS* chromosomal disruption, while the W478Y mutant was not. The steady state kinetic parameters for the pyrophosphate exchange reaction were determined for both the W434Y and wild-type ThrRS, employing a wider range of substrate concentrations than in our previously reported study (*22*). As shown in Table 2, moderate changes in both steady state parameters were noted. The k_{cat} for exchange was reduced by 2−3-fold for W434Y relative to that of the wild-type protein, while the K_M for threonine increased 4.5-fold. These relatively modest effects, coupled with the absence of evidence of protein instability, suggest that the W434Y mutation has a minimal effect on global protein structure. To assess the effect of the mutation

Table 2: Steady State Kinetic Parameters for W434Y ThrRS and WT ThrRS in the Pyrophosphate Exchange Assay

enzyme[a]	$k_{cat,thr}$ (s^{-1})[b]	$k_{cat,ATP}$ (s^{-1})	$K_{M,thr}$ (μM)	$K_{M,ATP}$ (μM)
WT ThrRS	90[c]	90	201	267
W434Y ThrRS	42	30	897	387

[a] The enzyme concentration was fixed at 10 nM. [b] The indicated substrate was titrated over a concentration range from 135 μM to 5 mM. The concentration of the other substrate was fixed at 5 mM. [c] All values were determined from the best fit of the data to the Henri−Michaelis−Menten equation.

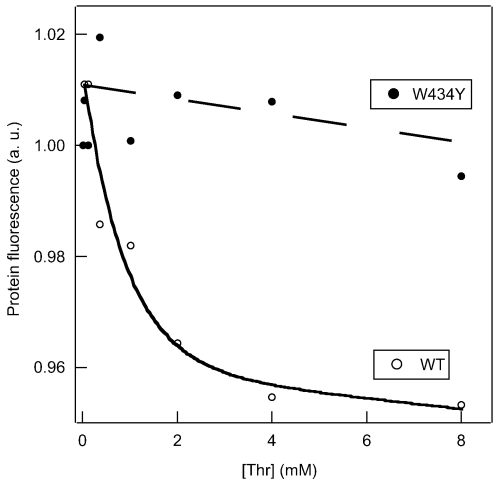

FIGURE 6: Effect of the W434Y substitution on total protein fluorescence. The plot shows a representative steady state threonine titration carried out in the presence of 0.5 μM enzyme: (○) WT ThrRS and (●) W434Y ThrRS. The amplitude of the solid line represents a 5% decrease in protein fluorescence, and the dashed line is a linear least-squares fit of W434Y data points.

on total enzyme fluorescence, steady state threonine titrations were carried out on both the wild-type and W434Y ThrRS. In the presence of the wild-type enzyme, the relative fluorescence decreased with increasing threonine concentration, and reached a maximum change of 5% (Figure 6). This is in excellent agreement with the pre-steady state results described above. In contrast, the W434Y mutant enzyme exhibited no fluorescence quench over a wide range (10 μM to 10 mM) of threonine concentrations. This suggests that Trp434 contributes significantly to the fluorescence changes observed upon incubation with substrates, and that a local structural element containing Trp434 undergoes a conformational change upon binding.

DISCUSSION

Development of a Kinetic Scheme To Describe ThrRS-Catalyzed Adenylation. Here, we have used changes in the intrinsic tryptophan fluorescence of ThrRS to follow the course of the adenylation reaction and develop a minimal kinetic model. These studies are based on the reversible fluorescence quench that accompanies the forward reaction, and the converse fluorescence increase that is equal in amplitude that accompanies the pyrophosphorolysis reaction. Table 1 summarizes the parameters that could be determined directly by measurement of the rates of the forward and reverse reactions as a function of substrate concentration, and those equilibrium constants that could be estimated by placing upper and lower limits on selected rate constants. The principal conclusion is that all of the reactions studied here could be analyzed in terms of a two-step mechanism whereby an initial binding step is followed by a subsequent isomerization step. For productive reactions involving threonine or β-HNV that were associated with adenylation chemistry, the binding step is faster than the subsequent chemical step, producing the characteristic hyperbolic response. With regard to the discrimination of noncognate substrates, it has been shown that the K_M for hydroxynorvaline, which has an ethyl group attached to the β-carbon (Figure 2), is only ~20 times greater than that of threonine. This analogue is efficiently misactivated, but is not encountered *in vivo* (*22*). Serine, on the other hand, has a K_M some 500-fold higher than that of threonine, in part because it cannot make hydrophobic contacts with Thr482 and Ala513 as does the methyl group of threonine (*22*), but this level of discrimination is not sufficient for elimination of the need for editing misactivated serine. Because of the extremely high concentrations that are necessary to saturate ThrRS with serine at the binding step, we have not yet been able to characterize its activation by pre-steady state kinetics.

Significantly, the nonproductive substrates all exhibited a linear dependence of k_{app} on ligand concentration. While the simplest explanation of a linear response is a simple bimolecular interaction, a linear response to an increasing S concentration can also be observed in a two-step mechanism if the bimolecular reaction is slow relative to the second step. This latter interpretation is supported by the observation that the overall amplitudes for both productive and nonproductive reactions (including those portions occurring within the dead time of the instrument) were equivalent, within the limits of experimental error. This is significant because it renders unlikely the idea that additional structural changes (expected to perturb the intrinsic enzyme fluorescence) occur following the formation of the isomerized, ThrRS[ES]* complex. Along these lines, we note that both the forward and reverse reactions were described well by single exponentials, which argues against the idea that pyrophosphate release is rate-limiting. We therefore suggest that in both types of reactions (productive and nonproductive substrates), the fluorescence changes are likely to be monitoring structural changes that immediately precede chemistry. The isomerization step is kinetically linked to chemistry for productive ligands, but is not linked in the case of nonproductive ligands. This argument receives additional, and independent, strong experimental support from a structural comparison of the ThrRS−Thr-AMS and bona fide ThrRS−threonyl-adenylate complexes, which indicate that the conformational changes associated with the productive and nonproductive ligands lead to the identical final state (see below). The fact that the final structures are similar says nothing about the rates of the conformational changes that lead to them, and our interpretation predicts that conformational changes should be faster for the nonproductive substrates (like threoninol and Thr-AMS) that do not undergo chemistry. A good precedent for this conclusion is found in the lysyl system, where the rates of the forward isomerization for productive substrates were in the range measured here (45 s^{-1}), while the nonproductive lysine amide substrate exhibited a much faster forward isomerization rate constant of 221 s^{-1} (*43*). Nevertheless, we must add a caveat to our interpretation by recalling that any mechanistic argument based largely on kinetics can never exclude more complicated mechanisms

that involve additional elementary steps and intermediates. Detecting such steps and intermediates would require additional probes of enzyme structure and mechanism that we do not currently possess.

An indication of the validity of a mechanistic scheme derived by pre-steady state kinetics is that it should be able to predict the corresponding steady state kinetics. In the threonyl system, this agreement is closest for ATP. The relationship between the overall dissociation constant and the specific dissociation constant from the E·Thr complex is as follows:

$$K_{\text{overall}} \cong K_{\text{M}} = \frac{K_3}{1 + \dfrac{k_{+5}}{k_{-5}}} \qquad (6)$$

By using the measured value of the dissociation constant for dissociation of ATP from the E·Thr complex and the values of k_{+5} and k_{-5}, a value for K_{overall} of 280 μM is obtained from eq 6, which is in good agreement with the steady state K_{M} of 267 μM (Table 2). This provides one independent confirmation of the validity of Scheme 1. The k_{cat} for pyrophosphate exchange is the rate of approach to equilibrium for [^{32}P]PP$_{\text{i}}$ exchanging into ATP. Accordingly, it should represent the sum of the forward and reverse rates of the rate-determining step of the adenylation reaction. The sum of the forward and reverse reactions ($k_{+5} + k_{-5}$) is 76 s^{-1}, which is close to the steady state measurement of 90 s^{-1} also determined here. As noted above, we do not rule out the possibility that a rate-determining conformational change precedes a very fast but optically invisible (with respect to fluorescence) chemical step in the presence of productive substrates. Rather, the interpretation presented here is the simplest one that is consistent with all the data.

The most significant discrepancy between the pre-steady state and steady state kinetics would appear to lie in the apparent equilibrium constant for threonine binding to the E·ATP complex determined in Figure 1C. By using the value of 1200 μM obtained from the midpoint of the titration in Figure 1C, and eq 4 (employing K_4 instead of K_3), a value of 677 μM can be estimated for the overall dissociation constant for threonine. This agrees poorly with the value of 201 μM determined for K_{M} by steady state kinetics (Table 2). This lack of agreement suggests that, for the case in which ATP binds first, threonine binding is not in rapid equilibrium relative to the isomerization step. Accordingly, fitting the data to eq 4 would be expected to produce a misleading result. Cases where the rapid equilibrium assumption breaks down have been treated by others (*49*, *53*). Under conditions where the rapid equilibrium assumption does not hold, the initial slope of the dependence of k_{app} on [Thr] can be taken to be an upper estimate of the effective rate of association (k_{+4} in this case), while the y intercept yields $(k_{-4}k_{-5})/(k_{+5} + k_{-5})$ (*49*, *53*). By eliminating the rapid equilibrium assumption and employing this analysis scheme, we found the initial slope yields a value of $(2.4 \pm 0.5) \times 10^4$ M^{-1} s^{-1} for k_{+4}, and approximately 2 s^{-1} for the intercept. The k_{+4} value for threonine is the same as k_{on} for threoninol determined above. Inserting the values for k_{+5} and k_{-5} determined above (29 and 47 s^{-1}, respectively) yields an upper limit for k_{-4} of approximately 3.2 s^{-1}. This, in turn, produces a smaller value of ~135 μM for the apparent dissociation constant for dissociation of threonine from the E·ATP complex, which is in much better agreement with the value of K_1 determined by equilibrium dialysis (Figure 5). The predicted K_{overall} for threonine from eq 6 is ~85 μM, somewhat lower than the K_{M} value of 110 μM measured previously using steady state methods (*22*). If the thermodynamic model of the system is sufficient, then $K_1K_3 = K_2K_4$ and a value of 717 μM can be inferred for K_2, the dissociation constant for dissociation of ATP from the free enzyme (Table 1). Taking these values as reasonable estimates of the four dissociation constants of threonine and ATP, we can consider substrate binding order random, and the prior binding of either threonine or ATP can be seen to decrease the dissociation constant of the second substrate. This interpretation would be consistent with the behavior of isoleucyl-tRNA synthetase, which is one of the few aminoacyl-tRNA synthetases whose pre-steady state kinetics have been investigated in depth (*34*).

Structural Changes Associated with Substrate Binding Mirror the Fluorescence Changes. In the *E. coli* ThrRS structure, Trp434 and Trp478 are both located in structural elements adjacent to substrate binding residues, but do not directly participate in substrate binding themselves (*21*, *22*). Here, we demonstrated that substitution of Trp434 with tyrosine simultaneously abolished the threonine-induced fluorescence quench and nearly half of the 10−13% overall fluorescence signal, while leaving threonine activation largely intact. Our biochemical and genetic evidence therefore argues in favor of a role in amino acid recognition for the local structural element in which Trp434 resides, a conclusion already evident from earlier crystallographic work (*21*, *22*) and explored in more detail below. In the ThrRS structure, Trp434 stabilizes the local hydrophobic core of a loop−helix−strand motif that forms the outer edge of the β-sheet structural core of the catalytic domain (*21*). This motif packs against a loop containing conserved active site residues such as Tyr462, which contacts the α-amino group of the threonine substrate. Thus, change in the local structure of this motif might well be expected to alter both the local environment of Trp434 (and therefore its fluorescent properties) and contact with the substrate. It is evident from the structure that W478 is the only other tryptophan that moves in response to the presence of substrate, and it is therefore likely to be responsible for the remaining 5−8% of the fluorescence signal observed here. W478 also stacks on M374 in the ATP-bound state, which may explain why the W478Y mutation results in a nonviable phenotype, *in vivo*. Mutagenesis at additional sites, including M374, will be required to confirm the role of this position in the intrinsic tryptophan fluorescence.

Two new structures of full-length ThrRS from *Staphylococcus aureus* complexed with Thr·ATP and with Thr-AMS have recently been reported, essentially completing the set of structures necessary for a full description of the ThrRS catalytic cycle (*54*). Comparison of these *S. aureus* complexes to those previously described for the *E. coli* enzyme (which include unliganded tRNA·AMP, Thr-AMS, and threonine alone complexes) indicates that ThrRS undergoes profound conformational changes in four distinct regions of the catalytic domain upon binding threonine and ATP, providing direct crystallographic evidence for the confor-

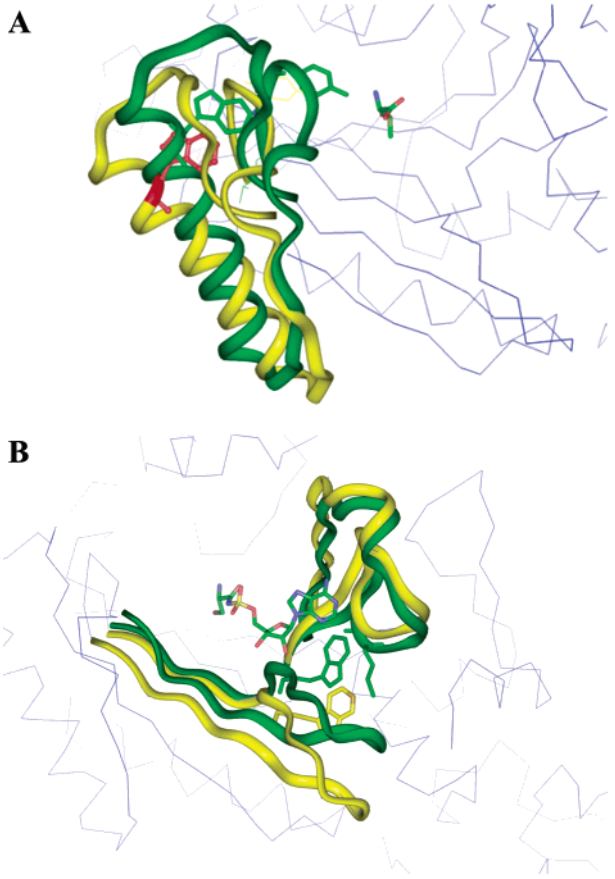

FIGURE 7: Effect of ligand-induced conformational changes on Trp434 and Trp478. Superimposed structures highlight changes in the positions of two mobile loops in the unliganded (yellow) and liganded (green) active site of *E. coli* WT ThrRS. A trace of alpha carbons in the catalytic domain is shown in cyan. (A) Movement of Trp434 in the catalytic site: unliganded position (red) and threonine-bound (green). (B) Stacking interaction between Trp478 and Met374 in the Thr-AMS-bound enzyme. The Thr-AMS ligand is stick-rendered in CPK coloring, and Trp478 is shown in its unliganded (yellow) and ligand-bound (green) conformations. Met374 is shown in the ligand-bound conformation.

mational changes we have proposed above. Two of these regions, namely, the motif 2 loop and the "flipping loop" (also termed the ordering loop), have been implicated in substrate-induced conformational changes in other class II complexes (*9*, *14*, *44*, *45*) and will not be discussed in detail here. The other two regions include the loop−helix−strand motif containing Trp434 described above, comprising a domain defined by residues 417−466 that moves in response to threonine binding (the "threonine loop"), and a region including residues 468−480 (the "ATP loop") that moves in response to ATP binding. Significantly, the former constitutes the loop−strand−helix motif where Trp434 is located, while the latter is the structural element in which Trp478 resides.

Figure 7 shows the effects of threonine binding, which include a 14° rotation in the threonine loop, and large conformational changes that alter the position of at least 50 different residues. This change has several notable consequences for the recognition of threonine and the mechanism of adenylation. First, it causes a 3 Å shift in the position of Tyr462, setting up the crucial contact with the α-amino group of threonine. It also leads to a similar displacement of Lys465, a threonine system conserved residue that, in the Thr−ATP complex, is positioned to neutralize developing negative charge on the α-phosphate during the adenylation reaction. Such a catalytic role is reminiscent of the catalytic Arg259 in HisRS (*45*). Last, the motion of the threonine binding domain brings it much closer to the ordering loop, which has the effect of closing the active site over the amino acid substrate. The conformational change in the threonine loop domain is seen in all threonine (and threonyl-adenylate) complexes relative to the apoenzyme, indicating that it is a consequence of threonine binding alone, and not ATP binding or adenylate formation. Because Trp434 plays a limited role (i.e., stacking interactions with aliphatic side chains Asp431 and Asp435, neither of which contacts the threonine substrate) in preserving the structure of the "threonine binding loop", the retention of adenylation function by the Trp434 to tyrosine substitution can be easily rationalized. It is interesting that the topologically equivalent regions of HisRS (*14*, *45*, *55*), LysRS (*10*, *11*), and ProRS (*14*) undergo closely related conformational changes upon binding their respective amino acids, indicating what is likely to be an emerging general feature of the class II mechanism.

In contrast to the conformational changes associated with threonine binding, the structural rearrangement in ThrRS that accompanies ATP binding appears at present to be specific to the threonine system. Binding of ATP by ThrRS is associated with an 8 Å shift in the position of the ATP loop (comprising residues 468−480), bringing the main chain carbonyl groups of residues 479 and 480 within hydrogen bonding range of the 2′- and 3′-hydroxyls of the ATP substrate. In addition to stabilizing interactions between ATP and the floor of the active site, this conformational change allows Trp478 to participate in a stacking interaction with Met374, fixing the position of motif 2, as well as moving Gln484 into position to potentially stabilize a coordinated Mg^{2+} ion between the β- and γ-phosphates of ATP. Consequently, the combined effect of threonine and ATP-induced conformational changes is to close the active site around these substrates, and bring essential catalytic groups into position to facilitate the adenylation reaction. The structural analysis illustrates that, by virtue of their fortuitous location within the threonine and ATP loops, Trp434 and Trp478 are ideally positioned to report on substrate-induced conformational changes. Thus, the crystallographic analysis indicates that, from a structural standpoint, ThrRS undergoes virtually identical conformation transitions in the presence of the productive substrates threonine and ATP, versus the product analogue Thr-AMS (*22*, *54*). While it is quite likely that other tryptophan residues in ThrRS contribute to the total intrinsic fluorescence signal, there is currently no evidence that any of them have a role in the transient signals associated with the forward or reverse adenylation reaction. Consistent with this view, the amplitudes of the fluorescent signals observed upon incubation of ThrRS lacking the N1,N2 editing domain (wherein reside four of the 11 tryptophans in the monomer) with threonine and ATP are, if anything, increased relative to that of the full-length enzyme (M. L. Bovee and C. S. Francklyn, unpublished observations).

Generality of the Induced Fit for Rate Enhancement by Aminoacyl-tRNA Synthetases. This work serves to underscore the importance of induced fit for the aminoacyl-tRNA synthetase (aaRS) catalytic mechanism, and provides an illustration of how pre-steady state kinetics can provide

information that is highly complementary to what is revealed by structure. Indeed, comparison of the example established by ThrRS to other well-studied class I and class II systems suggests that the dynamic features of induced fit provide a more accurate picture of aaRS function than earlier, more static, models featuring rather rigid amino acid and ATP binding pockets. A survey of those systems where both detailed kinetics and structural analysis have been conducted reinforces this point. Among the class II systems, considerable structural evidence suggests the importance of induced fit for the histidyl (*13*, *14*, *55*), prolyl (*14*), and lysyl (*11*, *56*, *57*) enzymes which, as described above for ThrRS, exhibit analogous amino acid-induced conformational changes. Notably, the pre-steady state kinetic analysis of LysRS was also interpreted as a two-step mechanism in which rapid equilibrium binding of lysine and ATP was followed by a unimolecular conformational change (*43*). In the aspartyl system, by contrast, the conformational changes associated with the adenylation reaction are much more limited, and largely confined to the flipping loop (*8*, *9*).

On the basis of pre-steady state kinetic and crystallographic studies on tyrosyl-tRNA synthetases, Fersht and colleagues argued that catalysis is achieved largely through the development of binding energy to the transition state and product complexes (*27*, *28*, *58*). Despite the limited structural data available at the time of the work, a key feature of their models is that interactions with tyrosine remain fixed during the reaction, while those with ATP undergo significant optimization as the transition state is approached. These additional interactions come at the expense of ground state binding interactions with ATP such that free energy is realized to drive conformational changes associated with induced fit (*32*). Fersht and colleagues also invoked a specific high-energy intermediate TyrRS·[Tyr·ATP] complex, which is analogous to the pre-transition state conformational change we have proposed here for ThrRS (*28*, *58*). More recently, Retailleau *et al.* (*59*) have confirmed and extended these proposals in crystallographic studies of the related class Ic tryptophanyl-tRNA synthetase (TrpRS). These authors described two structural forms of the TrpRS−ATP complex: the first being a high-affinity "open complex" and the second a low-affinity "closed complex". These structural data and other lines of evidence from kinetics suggest that tryptophan and ATP bind to the open complex in random order, followed by a subsequent conformational isomerization to the closed complex that is significantly destabilized with respect to ATP binding. These data provide noteworthy structural validation of Fersht's earlier proposals, and indicate that substantial free energy must be extracted from ATP binding to drive the conformational changes required to position ATP in the proper orientation for reaction with tryptophan. The generality of this concept for other class I enzymes is further suggested by recent structural analysis of the GluRS−$tRNA^{Glu}$−ATP ternary complex, in which the free energy for properly positioning the ATP is apparently derived from aaRS−tRNA interactions (*60*). In all cases, this principle rationalizes the observation that despite the extensive and comprehensive interactions that aaRSs make with their ATP and tRNA substrates, the binding constants are relatively weak. It can therefore be stated with some confidence that, although different synthetase systems employ a variety of specific mechanisms and particular structural changes, destabilization of ground state binding through conformation change is a principle that unifies the mechanism of both class I and class II systems. Indeed, this principle is a classic tenet of enzymology (*61*, *62*).

Induced Fit Does Not Obviate the Need for Editing. As significant as induced fit is in enforcing specificity at the level of adenylation, many systems require additional editing mechanisms for clearing amino acids that are smaller than cognates. A central feature of these systems is a requirement for the cognate transfer RNA, both for pretransfer strategies in which it causes the hydrolysis of the noncognate adenylate and for post-transfer mechanisms involving the formation of a transient misacylated tRNA whose 3′-end migrates to the editing site. The role of induced fit in these editing mechanisms is still emerging, but is likely to be important. In the threonyl system, induced fit promotes a conformational switch of several active site residues (e.g., Tyr462, Arg375, and Arg476) from recognition of ATP and threonine moieties in the first reaction to tRNA functional groups in the second reaction (*54*). Thus, by directly promoting interactions with the cognate tRNA, induced fit lays the foundation for tRNA-dependent editing activities as well. We would predict that in other class II systems that carry out editing, such as ProRS (*24*, *25*) and AlaRS (*26*), induced fit mechanisms are likely to contribute to interactions with the cognate tRNA.

ACKNOWLEDGMENT

We express our gratitude to Anne-Catherine Dock-Brégeon and other members of the laboratory of Dino Moras for communicating structural results in advance of publication, as well as providing the threonyl-adenylate analogue. We also thank Mathias Springer for providing numerous *thrS* bacterial strains. Collaborators Christopher Berger at the University of Vermont and Sriram Krishnaswamy at the Joseph Stokes Research Institute, Children's Hospital of Philadelphia (Philadelphia, PA), are gratefully acknowledged for instruction and the use of stopped flow fluorimeters, as well as extensive discussions. Thanks are also extended to John Weeks and Jozsef Urmos at WaveMetrics, Inc. (Lake Oswego, OR), for in-depth technical assistance with Igor graphing software.

REFERENCES

1. Ibba, M., and Söll, D. (2000) *Annu. Rev. Biochem. 69*, 617−650.
2. Arnez, J. G., and Moras, D. (1997) in *RNA Structure and Function* (Grunberg-Manago, M., and Symons, R. W., Eds.) Cold Spring Harbor Laboratory Press, Plainview, NY.
3. Webster, T. A., Tsai, H., Kula, M., Mackie, G., and Schimmel, P. (1984) *Science 226*, 1315−1317.
4. Eriani, G., Delarue, M., Poch, O., Gangloff, J., and Moras, D. (1990) *Nature 347*, 203−206.
5. Cusack, S. (1995) *Nat. Struct. Biol. 2*, 824−831.
6. Doring, V., Mootz, H. D., Nangle, L. A., Hendrickson, T. L., de Crecy-Lagard, V., Schimmel, P., and Marliere, P. (2001) *Science 292*, 501−504.
7. Brick, P., Bhat, T. N., and Blow, D. M. (1989) *J. Mol. Biol. 208*, 83−98.
8. Cavarelli, J., Eriani, G., Rees, B., Ruff, M., Boeglin, M., Mitschler, A., Martin, F., Gangloff, J., Thierry, J. C., and Moras, D. (1994) *EMBO J. 13*, 327−337.
9. Schmitt, E., Moulinier, L., Fujiwara, S., Imanaka, T., Thierry, J. C., and Moras, D. (1998) *EMBO J. 17*, 5227−5237.
10. Desogus, G., Todone, F., Brick, P., and Onesti, S. (2000) *Biochemistry 39*, 8418−8425.
11. Onesti, S., Desogus, G., Brevet, A., Chen, J., Plateau, P., Blanquet, S., and Brick, P. (2000) *Biochemistry 39*, 12853−12861.

12. Arnez, J. G., Harris, D. C., Mitschler, A., Rees, B., Francklyn, C. S., and Moras, D. (1995) *EMBO J. 14*, 4143−4155.
13. Åberg, A., Yaremchuk, A., Tukalo, M., Rasmussen, B., and Cusack, S. (1997) *Biochemistry 36*, 3084−3094.
14. Yaremchuk, A., Tukalo, M., Grotli, M., and Cusack, S. (2001) *J. Mol. Biol. 309*, 989−1002.
15. Pauling, L. (1958) *The probability of errors in the process of synthesis of protein molecules*, Birkhauser Verlag, Basel, Switzerland.
16. Baldwin, A. N., and Berg, P. (1966) *J. Biol. Chem. 241*, 839−845.
17. Schmidt, E., and Schimmel, P. (1994) *Science 264*, 265−267.
18. Loftfield, R. B., and Vanderjagt, M. A. (1972) *Biochem. J. 128*, 1353−1356.
19. Nureki, O., Vassylyev, D. G., Tateno, M., Shimada, A., Nakama, T., Fukai, S., Konno, M., Hendrickson, T. L., Schimmel, P., and Yokoyama, S. (1998) *Science 280*, 578−582.
20. Silvian, L. F., Wang, J., and Steitz, T. A. (1999) *Science 285*, 1074−1077.
21. Sankaranarayanan, R., Dock-Bregeon, A. C., Romby, P., Caillet, J., Springer, M., Rees, B., Ehresmann, C., Ehresmann, B., and Moras, D. (1999) *Cell 97*, 371−381.
22. Sankaranarayanan, R., Dock-Bregeon, A. C., Rees, B., Bovee, M., Caillet, J., Romby, P., Francklyn, C., and Moras, D. (2000) *Nat. Struct. Biol. 7*, 461−465.
23. Dock-Bregeon, A., Sankaranarayanan, R., Romby, P., Caillet, J., Springer, M., Rees, B., Francklyn, C. S., Ehresmann, C., and Moras, D. (2000) *Cell 103*, 877−884.
24. Beuning, P. J., and Musier-Forsyth, K. (2000) *Proc. Natl. Acad. Sci. U.S.A. 97*, 8916−8920.
25. Wong, F. C., Beuning, P. J., Nagan, M., Shiba, K., and Musier-Forsyth, K. (2002) *Biochemistry 41*, 7108−7115.
26. Beebe, K., Ribas De Pouplana, L., and Schimmel, P. (2003) *EMBO J. 22*, 668−675.
27. Wells, T. N. C., and Fersht, A. R. (1986) *Biochemistry 25*, 1881−1886.
28. Fersht, A. R. (1987) *Biochemistry 26*, 8031−8037.
29. Fersht, A. R., Knill-Jones, J. W., Bedouelle, H., and Winter, G. (1988) *Biochemistry 27*, 1581−1587.
30. First, E. A., and Fersht, A. R. (1993) *Biochemistry 32*, 13658−13663.
31. First, E. A., and Fersht, A. R. (1993) *Biochemistry 32*, 13651−13657.
32. First, E. A., and Fersht, A. R. (1993) *Biochemistry 32*, 13644−13650.
33. Holler, E., and Calvin, M. (1972) *Biochemistry 11*, 3741−3752.
34. Pope, A. J., Lapointe, J., Mensah, L., Benson, N., Brown, M. J., and Moore, K. J. (1998) *J. Biol. Chem. 273*, 31680−31690.
35. Pope, A. J., Moore, K. J., McVey, M., Mensah, L., Benson, N., Osbourne, N., Broom, N., Brown, M. J., and O'Hanlon, P. (1998) *J. Biol. Chem. 273*, 31691−31701.
36. Pope, A. J., McVey, M., Fantom, K., and Moore, K. J. (1998) *J. Biol. Chem. 273*, 31702−31706.
37. Trézéguet, V., Merle, M., Gandar, J. C., and Labouesse, B. (1983) *FEBS Lett. 157*, 210−214.
38. Trézéguet, V., Merle, M., Gandar, J. C., and Labouesse, B. (1986) *Biochemistry 25*, 7125−7136.
39. Merle, M., Trezeguet, V., Graves, P. V., Andrews, D., Muench, K. H., and Labouesse, B. (1986) *Biochemistry 25*, 1115−1123.
40. Hyafil, F., Jacques, Y., Fayat, G., Fromant, M., Dessen, P., and Blanquet, S. (1976) *Biochemistry 15*, 3678−3685.
41. Kakitani, M., Tonomura, B., and Hiromi, K. (1989) *Biochim. Biophys. Acta 996*, 76−81.
42. Bartmann, P., Hanke, T., and Holler, E. (1975) *Biochemistry 14*, 4777−4786.
43. Takita, T., Akita, E., Inouye, K., and Tonomura, B. (1998) *J. Biochem. 124*, 45−50.
44. Belrhali, H., Yaremchuk, A., Tukalo, M., Berthet-Colominas, C., Rasmussen, B., Bösecke, P., Diat, O., and Cusack, S. (1995) *Structure 3*, 341−352.
45. Arnez, J. G., Augustine, J. G., Moras, D., and Francklyn, C. S. (1997) *Proc. Natl. Acad. Sci. U.S.A. 94*, 7144−7149.
46. Arnez, J. G., and Moras, D. (1997) *Trends Biochem. Sci. 22*, 211−216.
47. Shiio, I., Miyajima, R., and Nakamori, S. (1970) *J. Biochem. 68*, 859−866.
48. Caillet, J., Nogueira, T., Masquida, B., Winter, F., Graffe, M., Dock-Brégeon, A.-C., Torres-Larios, A., Sankaranarayanan, R., Westhof, E., Ehresmann, B., Ehresmann, C., Romby, P., and Springer, M. (2002) *Mol. Microbiol. 47*, 961−974.
49. Hiromi, K. (1979) *Kinetics of Fast Enzyme Reactions: Theory and Practice*, John Wiley & Sons, New York.
50. Austin, J., and First, E. A. (2002) *J. Biol. Chem. 277*, 14812−14820.
51. Bagshaw, C. R., Eccleston, J. F., Eckstein, F., Goody, R. S., Gutfreund, H., and Trentham, D. R. (1974) *Biochem. J. 141*, 351−364.
52. Mayaux, J. F., Fayat, G., Fromant, M., Springer, M., Grunberg-Manago, M., and Blanquet, S. (1983) *Proc. Natl. Acad. Sci. U.S.A. 80*, 6152−6156.
53. Betz, A., Vlasuk, G. P., Bergum, P. W., and Krishnaswamy, S. (1997) *Biochemistry 36*, 181−191.
54. Torres-Larios, A., Sankaranarayanan, R., Rees, B., Dock-Bregeon, A.-C., and Moras, D. (2003) *J. Mol. Biol. 331*, 201−211.
55. Qiu, X., Janson, C. A., Blackburn, M. N., Chhohan, I. K., Hibbs, M., and Abdel-Meguid, S. S. (1999) *Biochemistry 38*, 12296−12304.
56. Onesti, S., Miller, A. D., and Brick, P. (1995) *Structure 3*, 163−176.
57. Takita, T., Nakagoshi, M., Inouye, K., and Tonomura, B. (2003) *J. Mol. Biol. 325*, 677−695.
58. Fersht, A. R. (1988) *Biochemistry 27*, 1577−1580.
59. Retailleau, P., Huang, X., Yin, Y., Hu, M., Weinreb, V., Vachette, P., Vonrhein, C., Bricogne, G., Roversi, P., Ilyin, V., and Carter, C. W., Jr. (2003) *J. Mol. Biol. 325*, 39−63.
60. Sekine, S., Nureki, O., Dubois, D. Y., Bernier, S., Chenevert, R., Lapointe, J., Vassylyev, D. G., and Yokoyama, S. (2003) *EMBO J. 22*, 676−688.
61. Jencks, W. P. (1975) *Adv. Enzymol. 43*, 219−410.
62. Fersht, A. R. (1999) *Structure and Mechanism in Protein Science: A Guide to Enzyme Catalysis and Protein Folding*, W. H. Freeman and Co., New York.

BI0355701